THE JOURNAL OF PHYSICAL CHEMISTRY C

Article

pubs.acs.org/JPCC

Atomistic Observation of the Lithiation and Delithiation Behaviors of Silicon Nanowires Using Reactive Molecular Dynamics Simulations

Hyun Jung,[†,‡] Minho Lee,[†] Byung Chul Yeo,[†] Kwang-Ryeol Lee,[†] and Sang Soo Han*[,†]

[†]Center for Computational Science, Korea Institute of Science and Technology (KIST), Hwarangno 14-gil 5, Seongbuk-gu, Seoul 136-791, Republic of Korea

[‡]Department of Physics, Hanyang University, 222 Wangsimni-ro, Seongdong-gu, Seoul 133-791, Republic of Korea

Supporting Information

ABSTRACT: For the practical use of silicon nanowires (Si NWs) as anodes for Li-ion batteries, understanding their lithiation and delithiation mechanisms at the atomic level is of critical importance. Here, we report the mechanisms for the lithiation and delithiation of Si NWs determined using a large-scale molecular dynamics (MD) simulation with a reactive force field (ReaxFF). The ReaxFF is developed in this work using first-principles calculations. Our ReaxFF-MD simulation shows that an anisotropic volume expansion behavior of Si NWs during lithiation is dependent on the surface structures of the Si NWs; however, the volumes of the fully lithiated Si NWs are almost identical irrespective of the surface structures. During the lithiation process, Li atoms penetrate into the lattices of the crystalline Si (*c*-Si) NWs preferentially along the ⟨110⟩ or ⟨112⟩ direction, and then the *c*-Si changes into amorphous Li_xSi (*a*-Li_xSi) phases due to the simultaneous breaking of Si−Si bonds as a result of the tensile stresses between Si atoms. Before the complete amorphization of the Si NWs, we observe the formation of silicene-like structures in the NWs that are eventually broken into low-coordinated components, such as dumbbells and isolated atoms. However, during delithiation of the Li_xSi NWs, we observe the formation of a small amount of *c*-Si nuclei in the *a*-Li_xSi matrix below a composition of $Li_{1.4}Si \approx Li_{1.5}Si$, in which the volume fraction of formed *c*-Si phases relies on the delithiation rate. We also demonstrate that the two-phase structure can be thermodynamically more favorable than the single-phase *a*-Li_xSi. We expect that our comprehensive understanding of the lithiation and delithiation mechanisms along with the developed ReaxFF for Li−Si systems will provide helpful guidelines in designing Si anodes to obtain better performing Li-ion batteries.

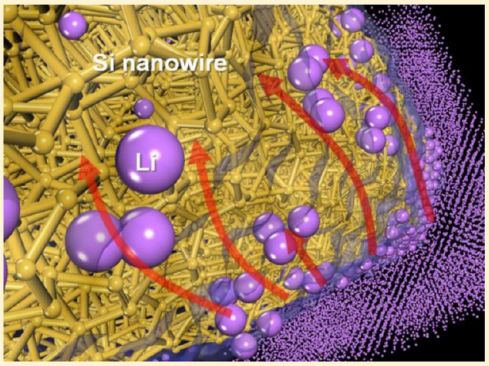

1. INTRODUCTION

Silicon (Si) has recently attracted considerable interest as a promising anode material for lithium (Li)-ion batteries due to its extremely high capacity of 4200 mAh/g (for $Li_{4.2}Si$), which is much higher than the value of 372 mAh/g (for LiC_6) for graphite.[1−4] However, Si seriously suffers from a large volume change (even up to 300%) of the electrode upon lithiation, leading to its destruction or mechanical failure during lithiation/delithiation processes followed by rapid capacity fading.[5−9] To overcome this problem, Si nanostructures, such as nanowires (NWs),[10,11] nanotubes,[12,13] nanoparticles,[14,15] and carbon-Si composites,[16,17] have been considered.

The lithiation mechanism for crystalline Si (*c*-Si) differs from that for graphite. In graphite, the Li atoms intercalate into the interlayer spaces between carbon sheets,[18] whereas in Si they occupy the interstitial sites (e.g., tetrahedral sites)[19−21] in the structure. During the lithiation process, *c*-Si undergoes a phase transformation to amorphous structures[4,15,22,23] even though the Li_xSi possesses several thermodynamically stable crystalline phases,[24] which indicates that the lithiation of Si is a nonequilibrium process. Additionally, the insertion of Li atoms into *c*-Si is faster along the ⟨110⟩ orientation than along other low-index orientations, which leads to a highly anisotropic volume expansion of the Si electrode.[23,25,26] Upon lithiation, the initially circular cross sections of nanopillars with ⟨100⟩, ⟨110⟩, and ⟨111⟩ axial orientations expand into cross, ellipse, and hexagonal shapes, respectively.[25,26] As indicated by these results, the lithiation mechanism for Si is very complex.

To design better Si electrodes, elucidating the atomic-scale mechanisms that include the volume expansion and the phase transformation that occur upon lithiation is critical. Several experimental and theoretical efforts to clarify the mechanism have been reported.[27−33] In particular, Liu et al.[27] found using *in situ* TEM that a sharp interface with a thickness of 1 nm exists between the *c*-Si and amorphous Li_xSi (*a*-Li_xSi) alloy. These authors suggested a dynamic ledge mechanism of lithiation-induced solid-state amorphization. Additionally, nuclear magnetic resonance (NMR) studies[28−30] revealed that the lithiation of Si leads to the breaking of Si−Si bonds to form small Si clusters and eventually isolated Si anions, and this result was supported by a first-principles molecular dynamics (MD) simulation.[31] However, using first-principles calculations,

Received: September 18, 2014
Revised: January 15, 2015
Published: January 30, 2015

DOI: 10.1021/jp5094756
J. Phys. Chem. C 2015, 119, 3447−3455

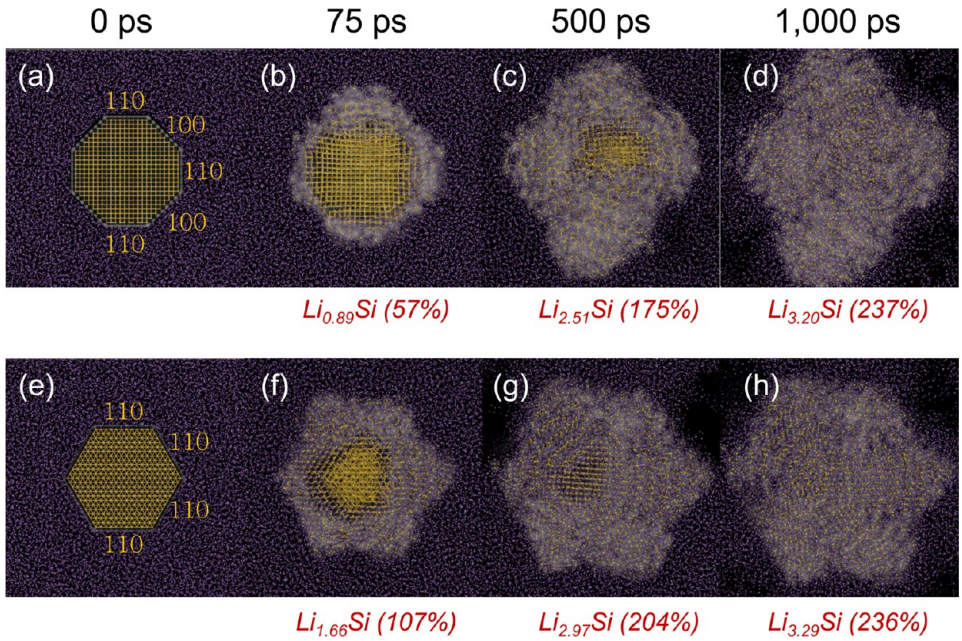

Figure 1. ReaxFF-MD snapshots for lithiation reactions of Si NWs. The top Si NW (a–d) has four (110) and four (100) surfaces, whereas the bottom Si NW (e–h) has six (110) surfaces. Color codes are yellow = Si and pink = Li. Additionally, the Li_xSi compositions and degrees of volume expansion are shown below each figure.

Wang et al.[32] found that local electron-rich conditions govern the electrochemically driven solid-state amorphization in Li_xSi alloys; however, Chan et al.[33] reported a solid-state amorphization in a Li_xSi alloy with no help from electrons using similar first-principles calculations. Moreover, using first-principles calculations, Zhao et al.[34] found that the insertion of Li into *c*-Si leads to continuous breaking of Si–Si bonds and to the formation of weaker bonds between neighboring Si and Li atoms, which accommodates the large plastic deformation of lithiated Si and then induces a phase transformation to amorphous Si structures.

Several theoretical works have been conducted to clarify the anisotropic volume expansion behavior of *c*-Si during lithiation. Jung et al.[35] calculated the equilibrium interfacial energies at the phase boundaries between *a*-Li_xSi and *c*-Si using first-principles calculations and reported that for the $Li_{3.4}Si$/Si interface, the (110) interfacial energy is smaller than that for other interfaces, such as (100) and (111), leading to a preferential volume expansion along the ⟨110⟩ direction. However, because the lithiation of Si is a nonequilibrium process, dynamic behaviors should be considered along with thermodynamics to obtain an accurate lithiation mechanism for Si. For this purpose, Cubuk et al.[36] used a multiscale method based on first-principles and kinetic Monte Carlo simulations to investigate the lithiation mechanism in Si NWs and reproduced the experimentally observed morphological changes of the Si NWs. In addition, using the finite element method, Yang et al.[37] showed that the anisotropic swelling of Si NWs during lithiation is critically controlled by the orientation-dependent mobility of interfaces between the *c*-Si core and the *a*-Li_xSi shell.

Compared to other simulation methods, MD simulations are very useful for studying atomic diffusion and phase transformations as functions of time at the atomic scale. Thus, this simulation method could provide detailed atomistic observations of lithiation in Si NWs, which have not yet been reported. However, for accurate predictions using MD simulations, it is critical to obtain a force field to appropriately describe the chemical reactions between Si and Li.

In this work, we develop a reactive force field (ReaxFF) for the Li–Si system based on quantum mechanical results and then perform large-scale MD simulations (approximately 100,000 atoms) to atomistically investigate the lithiation mechanism for Si NWs, including the anomalous shape change of the NWs during the lithiation process. Indeed, our simulations well reproduce the experimental phenomena and reveal a transient formation of silicene-like structures during the lithiation process, which has not yet been reported. Also, delithiation behaviors of Si NWs are discussed. Here, we note for nonexperts on batteries that lithiation of a Si anode occurs during the battery discharge and delithiation occurs during the battery charge.

2. COMPUTATIONAL DETAILS

To simulate the lithiation process in Si NWs, we employed molecular dynamics (MD) simulations with the ReaxFF,[38,39] which have successfully simulated chemical reactions in several systems, such as metals, ceramics, and organic compounds.[40−43] In this work, we independently developed the ReaxFF for Li–Si systems based on first-principles calculations, although another research group[44] recently reported the ReaxFF for this system to study the mechanical properties of *a*-Li_xSi alloys. Additionally, another research group[45] used the ReaxFF developed in ref 44 to investigate atomistic mechanisms of phase boundary evolution during the initial lithiation of *c*-Si. Details regarding the development of the ReaxFF can be found in the Supporting Information.

With the developed Li–Si ReaxFF, we performed MD simulations to investigate the lithiation/delithiation behaviors in Si NWs at the atomic level, using the LAMMPS[46] software with a Verlet[47] integration time step of 0.5 fs (femtosecond). The simulations were run in a canonical NVT ensemble at 300 K, in which the temperature was maintained by a Nosé–Hoover thermostat[48] with a damping parameter of 0.01 fs^{-1}.

DOI: 10.1021/jp5094756
J. Phys. Chem. C 2015, 119, 3447−3455

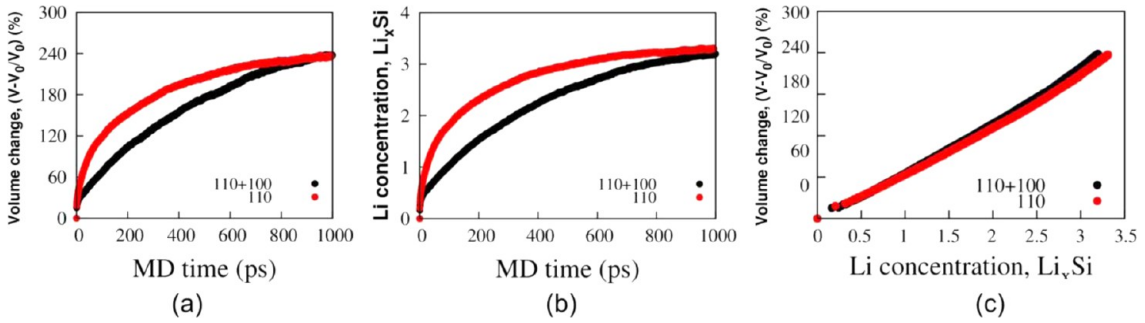

Figure 2. (a) Volume changes and (b) Li concentration profiles of Si NWs during lithiation, obtained from the ReaxFF-MD simulations presented in Figure 1. (c) Plot of the volume change versus Li concentration. Color codes are black = Si NW with six (110) surfaces and red = Si NW with four (110) and four (100) surfaces.

To clarify the anomalous volume expansion of Si NWs during lithiation, we considered two Si NWs with different surface structures, as previously investigated in experiments:[25,26] one has four (110) and four (100) surfaces, and the other has six (110) surfaces. The Si NWs, which had a diameter of ∼5 nm and a length of ∼10 nm, were immersed in a simulation cell with dimensions of 105.2 Å × 105.2 Å × 97.8 Å that was filled with Li atoms, and the Li atoms overlapping in the Si NWs were removed. The total number of atoms in the system was approximately 100,000. For modeling the Si NWs, we used the lattice parameter (5.47 Å) of bulk Si obtained from a DFT calculation and the 1 × 1 reconstruction for the surfaces of modeled Si NWs because surface Si dimers transform to a 1 × 1 reconstruction as the Li coverage increases.[49] Furthermore, a periodic boundary condition was applied along the *x*, *y*, and *z* directions during the MD simulations in which the axis of the NW is the *z* direction, leading to lithiation of the Si NWs along the *x* and *y* directions. Functionalization (−H, −O, and −OH and so on) of the dangling atoms on the Si surfaces could affect the lithiation reactions. This remains as our future work along with a development of ReaxFF for Si/O/H/Li systems.

3. RESULTS AND DISCUSSION

3.1. Anisotropic Volume Expansion of Si NWs during Lithiation. To investigate the anisotropic volume expansion behavior of Si NWs during lithiation, we considered two different structures of Si NWs: one that has four (110) and four (100) surfaces and another that has six (110) surfaces. Figure 1 shows the lithiation behaviors of the Si NWs. It is clear that Li atoms penetrate into the lattices of Si NWs, and then *a*-Li_xSi phases are formed in which core−shell structures of *c*-Si and *a*-Li_xSi are observed during the early stage of lithiation. As the lithiation proceeds, the *c*-Si phases continuously decrease. After 1000 ps, the volume of the Si NWs is significantly expanded by 240% for both structures of the Si NWs. Additionally, it is clearly observed that the two Si NWs exhibit different volume expansion behaviors. The Si NW that has four (110) and four (100) surfaces shows a 4-fold symmetrical volume expansion, and the Si NW that has six (110) surfaces shows a uniform volume expansion, which is consistent with previous experimental observations.[25,26] This anomalous volume expansion occurs because Li diffusion along the ⟨110⟩ direction of the Si NWs is faster than that along other directions. From these results, we can hypothesize that MD simulations using the ReaxFF for Li−Si developed in this work would reasonably predict the lithiation behaviors of Si materials.

The faster penetration of Li atoms along the ⟨110⟩ direction than along the ⟨100⟩ and ⟨111⟩ directions can be explained by the entrance area on the Si surfaces, through which Li diffuses into subsurfaces. The diffusion barrier for the surface penetration of Li primarily depends on the entrance area,[49] where a wider entrance provides easier penetration. As shown in Figure S5, Supporting Information, the (110) surface has the largest entrance area (20.9 $Å^2$/Si), whereas the (100) and (111) surfaces have entrance areas of 14.8 and 3.7 $Å^2$/Si, respectively.

Figure 2 shows the dependency of the lithiation rate on the Si surfaces. The Si NW with six (110) surfaces leads to faster lithiation than that with (110) and (100) surfaces, although both of the NWs eventually experience similar degrees of volume expansion. In other words, the volumes of the fully lithiated Si NWs are almost identical irrespective of the types of Si surfaces. Additionally, the Li concentration in Li_xSi formed during the lithiation process shows a similar behavior to the volume expansion. Thus, one can observe an almost linear relationship between the Li concentration and the degree of volume expansion, which was also previously demonstrated using the DFT calculations.[31,33,50]

The phase transformation of *c*-Si into *a*-Li_xSi during lithiation was further investigated using radial distribution function (RDF) analyses for Si−Si and Li−Si pairs (Figure 3), where the RDF is defined as the number of neighbors of a given species per unit volume as a function of distance. For the Si−Si

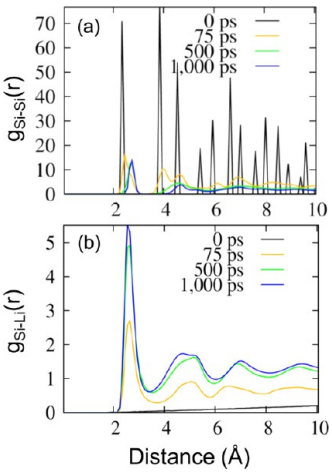

Figure 3. RDF *g*(*r*) analyses for (a) Si−Si and (b) Li−Si pairs in the Si NW with (110) and (100) surfaces during lithiation, which are obtained from the ReaxFF−MD simulations presented in Figure 1.

DOI: 10.1021/jp5094756
J. Phys. Chem. C 2015, 119, 3447−3455

pair, the initial structure of the Si NWs (0 ps) shows sharp peaks at 2.4, 3.9, and 4.6 Å, which correspond to the distances of the first, second, and third nearest neighbors between two Si atoms in the *c*-Si phase, respectively. As the number of MD steps increases and the lithiation thus proceeds further, the intensities of the peaks significantly decrease and the peaks shift to higher values, which clearly indicate a decrease in the crystallinity of the Si NWs and the evolution of amorphous phases. The first peak of the Si−Si pair located at 2.4 Å shifts to 2.8 Å after 1000 ps, which indicates that the amorphous phase has longer Si−Si bond distances than the crystalline phase.

In the RDF for Li−Si, there is no noticeable peak at 0 ps; however, as the MD time increases, several peaks are created. In particular, the intensity of the peak located at 2.6 Å increases with the MD time step, which clearly shows that the interaction between Si and Li atoms increases as the lithiation proceeds.

During lithiation, the *c*-Si phase transforms into the *a*-Li_xSi phase, in which interfaces between *c*-Si and *a*-Li_xSi exist. According to a high-resolution TEM study,[27] the width of the interface is approximately 1 nm. We analyzed the Li concentration distributions in the Si NWs along the ⟨110⟩ direction with the MD time step in Figure S6, Supporting Information, and a gradient interface with a thickness of approximately 1 nm was observed between the *c*-Si and *a*-Li_xSi in Figure 4. This result supports the reliability of our simulation using the ReaxFF developed in this work.

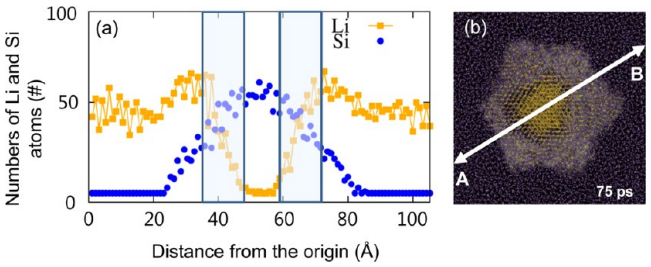

Figure 4. Concentration profiles (a) of Li and Si atoms in the Si NW along lines A and B in panel b. Here, the interfaces between *c*-Si and *a*-Li_xSi phases are shown in gray, indicating that their width is approximately 1 nm.

Figure 5 shows the residual stress distributions of the Si atoms in the radial direction (σ_r) during a lithiation process. The residual stress was obtained by averaging the atomic stress in the concentric shell between r and $r + \delta r$, where r is the radial distance from the center of the NW. At 0 ps, the Si atoms in the *c*-Si NW have almost zero stresses, although tension (positive value) and compression (negative value) regions exist near the surfaces of the NWs because the stress near the surface is relaxed by the atomic rearrangement. As the lithiation of the Si NWs proceeds, an *a*-Li_xSi phase evolves and then a *c*-Si/*a*-Li_xSi core−shell structure is formed (Figure 1). At 75 ps (the core−shell structure can be observed), the *c*-Si and *a*-Li_xSi phases have tensile stresses. Additionally, we can observe a compressive stress region with a width of 1 nm between the *c*-Si and *a*-Li_xSi phases, which can be regarded as an interface of the *c*-Si/*a*-Li_xSi. To form the *a*-Li_xSi phase, Si−Si bonds must be broken, which means that Si atoms have tensile stresses. The remaining *c*-Si phase in the core−shell structure has a longer Si−Si bond distance than that in the initial *c*-Si NWs, which can be found in the RDF presented in Figure 3, in which the first Si−Si peak shifts to a longer distance after a 75 ps MD

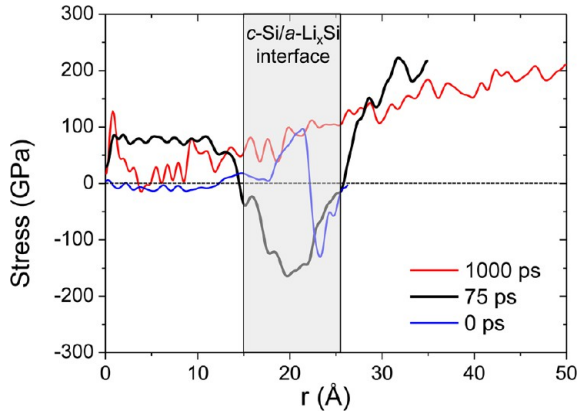

Figure 5. Residual stress distributions of Si atoms in the radial direction during lithiation. For 75 ps, one can observe a region of 1 nm with compressive stress (gray), which is an interface between the *c*-Si and *a*-Li_xSi core−shell structure.

simulation. Thus, the remaining *c*-Si phase in the core−shell structure also has a tensile stress. The interface of 1 nm with a compressive stress plays a role as a buffer layer to maintain two tension regions in *c*-Si and *a*-Li_xSi. However, at 1000 ps, the *c*-Si phase almost disappears, and instead, only the *a*-Li_xSi phase is found, which indicates that a tensile stress is dominant in the *a*-Li_xSi NWs. Figures 4 and 5 definitely show that a reactive MD simulation can be useful in assisting relevant experimental researches.

3.2. Atomistic Investigation on the Lithiation Mechanism for Si NWs. Using ReaxFF-MD simulations, we further investigated the lithiation behaviors in Si NWs to clarify the lithiation mechanism. Figure 6 shows an atomistic lithiation process of a Si NW taken during MD simulations. Li atoms preferentially penetrate Si surfaces along the ⟨110⟩ or ⟨112⟩ directions, where the penetration of Li atoms leads to the breaking of Si−Si bonds. It is clear that more lithiation in a Si NW breaks more Si−Si bonds. As the lithiation proceeds, the 6-membered rings of Si atoms in the initial Si NWs (Figure 6a) become low-coordinated components such as isolated atoms and small clusters (Figure 6e), where the lithiated Si NWs obtained after MD simulations of 1000 ps have the $Li_{3.2-3.3}Si$ composition as shown in Figure 1. More lithiation into the lithiated Si NWs would lead to further breaking of the small Si clusters. According to the NMR experiments,[28−30] lithiation of *c*-Si progresses with bond breakage of the Si matrix from the surface by forming both lithiated isolated Si atoms and small clusters (of 2−5 Si atoms). This is followed by breakage of the remaining Si clusters to form predominantly fully lithiated isolated Si environments, indicating that the fully lithiated phase with the $Li_{3.75}Si$ composition has only isolated Si atoms. Here, we can definitely confirm that our MD simulation results are similar to the NMR experiments.

Interestingly, we found that during the lithiation of Si NWs silicene (the Si counterpart of graphene)-like structures are formed, as shown in Figure 7. The formation of silicene-like structures was observed in the MD time range of 150−450 ps. This result provides a key for understanding the lithiation mechanism for Si NWs. As Li atoms penetrate into the Si NWs along the A direction in Figure 8a, the chemical bonds between two Si atoms (e.g., 1 and 2) break. The penetration of additional Li atoms along the B direction in Figure 8a leads to the breaking of bonds between Si atoms (e.g., 3 and 4). Further

DOI: 10.1021/jp5094756
J. Phys. Chem. C 2015, 119, 3447−3455

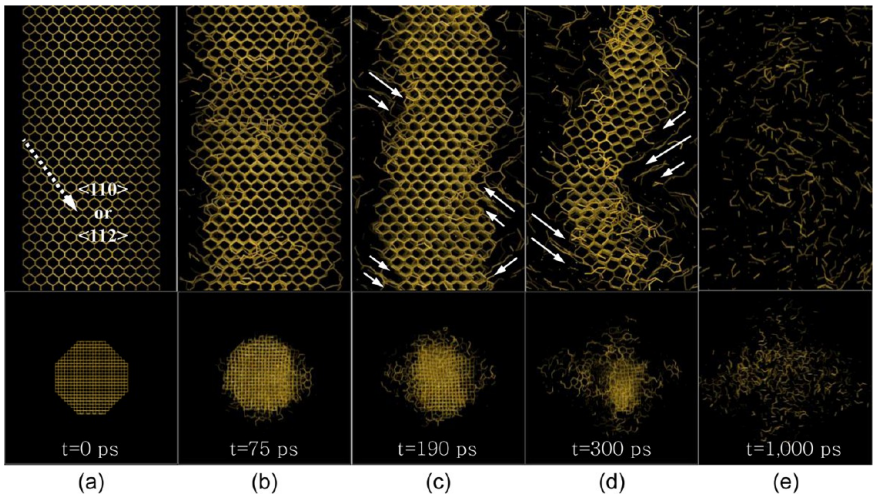

Figure 6. Lithiation mechanism for a Si NW. Li atoms penetrate into the lattices of *c*-Si preferentially along the ⟨110⟩ or ⟨112⟩ direction. Top and bottom figures present side and top views, respectively. Arrows in panels c and d show the directions of Li penetration. Here, Li atoms are excluded to improve the clarity.

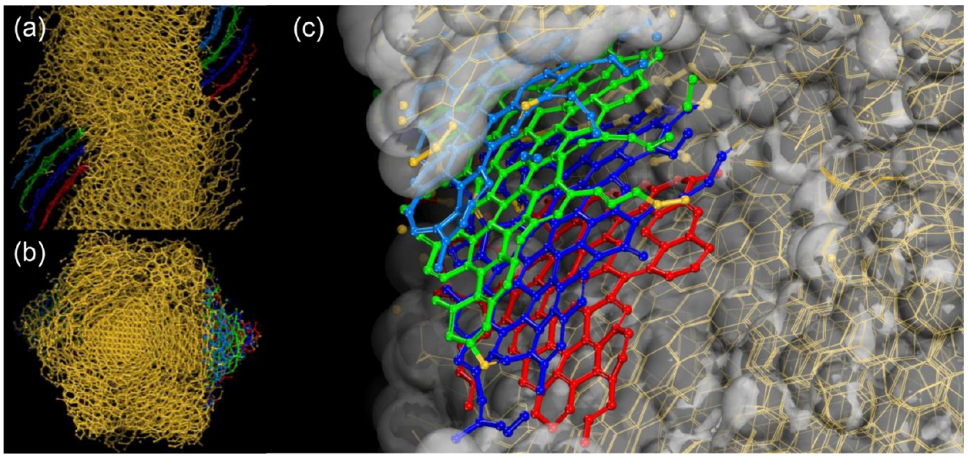

Figure 7. Formation of silicene-like structures (cyan, green, blue, and red sheets) in Si NWs during lithiation, where Li atoms are excluded to improve the clarity. (a,b) Side and top views of lithiated Si NWs, respectively, and (c) enlarged view of panle a for clarifying formation of silicene-like structures.

Li penetration along the A or B direction leads to additional breaking of Si−Si bonds, subsequently leading to the formation of silicene-like structures, which are highlighted with a yellow color in Figure 8a. The formation of silicene-like structures is transient. Eventually, the structures are broken and become low-coordinated components, such as dumbbells and isolated atoms. The lithiation mechanism for Si NWs determined in this work is similar to the ledge mechanism proposed in an in situ TEM study;[27] however, the experiment did not directly observe the formation of silicene-like structures because their formation might be very transient. This indicates that the ReaxFF-MD simulation can be effectively used to clarify the lithiation mechanism of Si NWs along with experiments.

3.3. Delithiation Process of the Lithiated Si NWs. In addition to the lithiation process of Si NWs, the delithiation behavior is also very critical for their battery performances. However, most previous theoretical works on the properties of Si NWs for lithium-ion batteries focused on the lithiation process. It is technically challenging to investigate the delithiation process using a theoretical method at the atomic level. However, with the reactive molecular dynamics simulation employed in this work, one can investigate the delithiation process of lithiated Li_xSi NWs.

To simulate the delithiation process (Figure S7, Supporting Information), we have an assumption that Li atoms near Si surfaces first escape out the Si electrode during an experimental delithiation process. We considered the "thin" shell of the Li_xSi NW with a thickness of 5 Å and removed all of the Li atoms inside the shell. We also removed all Li atoms in the surrounding fluid. Then, we obtained the core−shell structure of the Li_xSi NW where Li atoms exist only in the core, leading to a gradient of Li concentrations between the core and shell. To relax the core−shell structure, we performed a MD simulation, which provides the redistribution of Li concentration. This process is defined as the first step. Then, we considered the shell of the Li_xSi NW obtained after the first step and repeat the processes such as Li removal and MD simulation explained in the first step, which is the second step. If one repeats this process 10 times, the volume and Li concentration of Li_xSi approaches to almost constant values. Here, one can describe different delithiation rates by considering a different shell thickness or a MD simulation time.

The detail algorithm is explained below:

DOI: 10.1021/jp5094756
J. Phys. Chem. C 2015, 119, 3447−3455

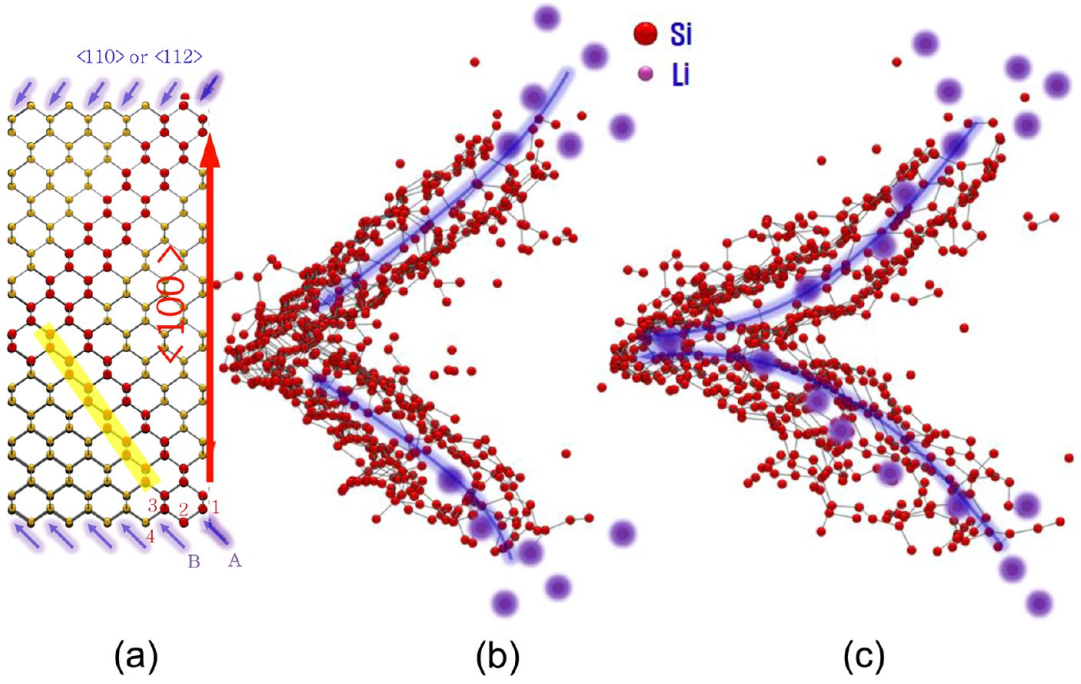

Figure 8. ReaxFF-MD snapshots of lithiation of Si NWs obtained after MD simulations of (a) 0, (b) 310, and (c) 500 ps. The yellow in panel a indicates a silicene structure.

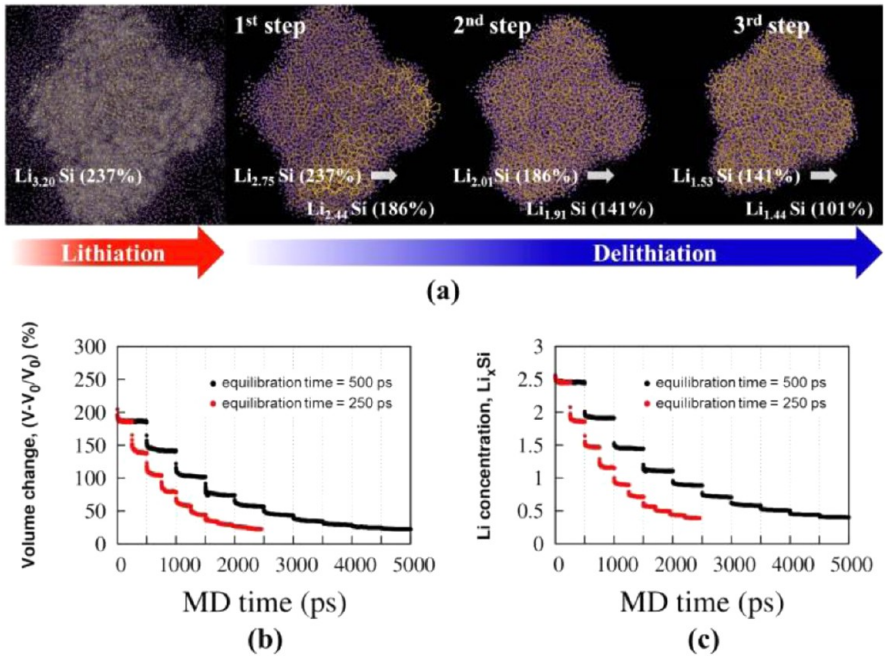

Figure 9. (a) ReaxFF-MD snapshots for the delithiation process of a lithiated Si NW; (b) volume change of the lithiated Si NW during delithiation, which is relative to the initial *c*-Si NW shown in Figure 1; and (c) Li concentration change in the lithiated Si NW during delithiation. Black and red colors in panels b amd c indicate results obtained with MD equilibrations of 500 and 250 ps for each delithiation step, respectively.

(1) As an initial model for the delithiation of a Li_xSi NW, the Li_xSi NW obtained after a 1000 ps MD for the lithiation was considered (e.g., the first figure in Figure 9a). The Si NW with both (110) and (100) surfaces had a $Li_{3.20}Si$ composition with a volume expansion of 237%.

(2) In the $Li_{3.20}Si$ NW, the Li atoms inside the shell with a thickness of 5 Å were removed, which led to the $Li_{2.75}Si$ NW with a volume expansion of 237% (the second figure in Figure 9a). Here, Li atoms remaining in the sea of Li (Li atoms located outside of the Li_xSi NW) were also removed.

(3) The Si NW with a reduced Li concentration ($Li_{2.75}Si$) was equilibrated for 500 ps. From the MD equilibration, the volume of the NW was decreased from 237% to 186%, which can be called the first step of the delithiation process (the second figure in Figure 9a). For a comparison, we also considered a MD equilibration time of 250 ps.

DOI: 10.1021/jp5094756
J. Phys. Chem. C 2015, 119, 3447−3455

(4) Processes 2 and 3 were repeated, which is the second step of the delithiation process (the third figure in Figure 9a).
(5) The process was repeated ten times.

Figure 9 shows the delithiation process of the Li_xSi NW obtained using the above algorithm. During the delithiation process, the volume of the Li_xSi is decreased from 240% relative to the *c*-Si NW to 25%. Simultaneously, the composition of the Li_xSi is decreased from $Li_{3.2}Si$ to $Li_{0.5}Si$.

Note that during the delithiation process a small number of crystalline Si nuclei are formed (Figures 10 and S8, Supporting Information), although most of the delithiated Si NWs show an amorphous structure, which was previously observed in several experiments.[51−54] A RDF analysis for the Si−Si pair in Figure 10 shows that the peaks for *c*-Si (e.g., 2.4 Å) are created during delithiation and that the peak intensity continuously increases as the delithiation proceeds. During our simulation, the recrystallization of a Si NW was observed after the third delithiation step (1000−1500 ps), indicating that the phenomenon could be observed below a composition of approximately $Li_{1.4}Si \approx Li_{1.5}Si$.

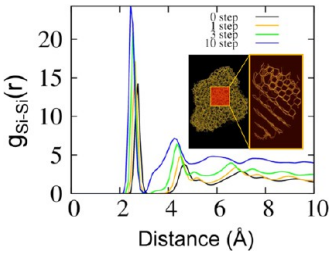

Figure 10. RDF $g(r)$ for the Si−Si pair in the lithiated Si NW during the delithiation process, obtained from the MD simulations presented in Figure 9. The inset shows the formation of *c*-Si nuclei in the Li_xSi NW after the 3rd step of delithiation, where Li atoms are excluded to improve the clarity.

The recrystallization of Si NWs can be thermodynamically possible. In other words, the two-phase structure with *c*-Si and *a*-Li_xSi could be more stable than a single-phase structure of *a*-Li_xSi with an overall uniform Li content. The energy for the formation of the *a*-Li_xSi structure relative to bulk *c*-Si and bcc Li negatively increases (thermodynamically more favorable) with the Li content up to approximately $x = 4.0$, where the energies for the pure *c*-Si and bcc Li are zero (see Figure S9, Supporting Information).[24,50,54] Assume that the formation energy for the single-phase *a*-Li_xSi with $x = x_1$ is E_1 and that the volume fractions of *c*-Si and *a*-Li_xSi in the two-phase structure are V_c and V_a ($V_c = 1 - V_a$), respectively. Here, *a*-Li_xSi in the two-phase structure has a Li content of $x = x_2$ ($x_2 > x_1$), because both of the single- and two-phase structures have the same average Li concentration (i.e., $x_1 = V_a x_2$). The formation energy for the two-phase structure can be expressed as V_aE_2 because the energy for pure *c*-Si is zero. For the two-phase structure to be themodynamically more stable than the single-phase structure, the following condition must be satisfied:

$V_aE_2 < E_1$, where $E_2 < E_1$ and both E_1 and E_2 are negative values.

Then, $V_a > E_1/E_2$, where $E_1/E_2 < 1$.

Therefore, $V_c = 1 - V_a < 1 - E_1/E_2$.

Here, V_c must have a positive value in the range from 0 to 1. This is physically correct, which clearly indicates that the formation of *c*-Si in the two-phase structure is thermodynamically possible.

We additionally performed DFT calculations for a single-phase structure of *a*-Li_xSi and a two-phase structure with *c*-Si and *a*-Li_xSi, where the two cases have the same Li concentration of $Li_{1.4}Si$ with 90 Li atoms and 64 Si atoms. Indeed, the DFT calculation shown in Figure S10, Supporting Information, shows that the two-phase structure is more stable by 14 meV/Si than the single-phase structure, which supports our ReaxFF result and relevant argument.

In order to investigate effects of a delithiation rate on the stability of the two-phase structure with *c*-Si and *a*-Li_xSi, we also considered a MD equilibration time of 250 ps for each delithiation step (red in Figure 9b,c) to simulate a faster delithiation rate. A simulation using the equilibration of 250 ps also shows formation of two-phase structures; however, the volume fraction (V_c) of *c*-Si phases formed in the two-phase structure is lower than that obtained with a slower rate because a faster delithiation rate allows a shorter time to form the *c*-Si phase. Indeed, our simulations using MD equilibration times of 500 and 250 ps show the V_c of 13% and 7%, respectively, after the 10th step of delithiation. This clearly indicates that the evolution of the two-phase structure relies on the delithiation rate.

4. CONCLUSION

Using MD simulations with the ReaxFF developed in this work, we find that an anisotropic volume expansion behavior of Si NWs during lithiation is dependent on the surface structures of the Si NWs; however, the volumes of the fully lithiated Si NWs are almost identical irrespective of the surface structures. During the lithiation process, Li atoms penetrate into the lattices of the *c*-Si NWs preferentially along the ⟨110⟩ or ⟨112⟩ direction, and then the *c*-Si transforms to *a*-Li_xSi phases due to the simultaneous breaking of Si−Si bonds. We also observed the formation of silicene-like structures in Si NWs during lithiation, which provides a new approach for the silicene synthesis. In other words, silicene can be readily obtained by the electrochemical lithiation process of Si NWs.

During the delithiation of the Li_xSi NWs, a small amount of *c*-Si nuclei can be formed in the *a*-Li_xSi matrix, where the slower delithiation rate leads to the more formation of the *c*-Si. This also indicates that the Si structures smaller in size are more favorable for the recrystallization of *c*-Si phase because Si atoms in the smaller structures can move more freely to form their crystalline phases. Thus, if one synthesizes Si nanostructures as small as possible (e.g., very thin nanosheet), the Si material could show an improved cyclic property due to more recrystallization of *c*-Si during the delithiation process.

We expect that our comprehensive understanding of the lithiation and delithiation mechanisms for Si NWs will provide insight for the future design of improved Si-based anodes for Li-ion battery applications. Furthermore, the ReaxFF developed in this work can be widely used in predicting battery performances for newly designed Si-based electrodes. In particular, after additional ReaxFF development for carbon and oxygen, one can study the lithiation and delithiation behaviors of various Si/C composites (e.g., core−shell heterostructures, depositing Si−C multilayer films, and C coating on Si nanowires and nanotubes) and SiO_x materials, at the atomic scale. For example, one future work is to design structures of optimum carbon coating of Si or SiO_x active materials.

DOI: 10.1021/jp5094756
J. Phys. Chem. C 2015, 119, 3447−3455

■ ASSOCIATED CONTENT

Supporting Information

Details regarding development of ReaxFF and additional results regarding lithiation and delithiation of Si NWs. This material is available free of charge via the Internet at http://pubs.acs.org.

■ AUTHOR INFORMATION

Corresponding Author

*E-mail: sangsoo@kist.re.kr. Tel: +82 2 958 5441. Fax: +82 2 958 5451.

Notes

The authors declare no competing financial interest.

■ ACKNOWLEDGMENTS

We thank the financial supports from the Korea Institute of Science and Technology (Grant No. 2E24630) and from the Industrial Strategic Technology Development Program (Grant No. 10041589) funded by the Ministry of Trade, Industry, and Energy (MOTIE) of Korea. This work was supported by the National Research Foundation of Korea Grant funded by the Korean Government (MSIP) (NRF-2011-C1AAA001-0030538).

■ REFERENCES

(1) Kasavajjula, U.; Wang, C. S.; Appleby, A. J. Nano- and Bulk-Silicon-Based Insertion Anodes for Lithium-Ion Secondary Cells. *J. Power Sources* **2007**, *163*, 1003−1039.

(2) Obrovac, M. N.; Christensen, L. Structural Changes in Silicon Anodes during Lithium Insertion/Extraction. *Electrochem. Solid-Sate Lett.* **2004**, *7*, A93−A96.

(3) Obrovac, M. N.; Krause, L. J. Reversible Cycling of Crystalline Silicon Powder. *J. Electrochem. Soc.* **2007**, *154*, A103−A108.

(4) Liu, X. H.; Zhang, L. Q.; Zhong, L.; Liu, Y.; Zheng, H.; Wang, J. W.; Cho, J.-H.; Dayeh, S. A.; Picraux, S. T.; Sullivan, J. P.; et al. Ultrafast Electrochemical Lithiation of Individual Si Nanowire Anodes. *Nano Lett.* **2011**, *11*, 2251−2258.

(5) Ng, S.; Wang, J.; Wexler, D.; Konstantinov, K.; Guo, Z.; Liu, H. Highly Reversible Lithium Storage in Spheroidal Carbon-Coated Silicon Nanocomposites as Anodes for Lithium-Ion Batteries. *Angew. Chem., Int. Ed.* **2006**, *45*, 6896−6899.

(6) Larcher, D.; Beattie, S.; Morcrette, M.; Edstroem, K.; Jumas, J.-C.; Tarascon, J.-M. Recent Findings and Prospects in the Field of Pure Metals as Negative Electrodes for Li-Ion Batteries. *J. Mater. Chem.* **2007**, *17*, 3759−3772.

(7) Zhou, S.; Liu, X. H.; Wang, D. W. Si/$TiSi_2$ Heteronanostructures as High-Capacity Anode Material for Li Ion Batteries. *Nano Lett.* **2010**, *10*, 860−863.

(8) McDowell, M. T.; Lee, S. W.; Wang, C.; Cui, Y. The Effect of Metallic Coatings and Crystallinity on the Volume Expansion of Silicon during Electrochemical Lithiation/Delithiation. *Nano Energy* **2012**, *1*, 401−410.

(9) Yao, Y.; McDowell, M. T.; Ryu, L.; Wu, H.; Liu, N.; Hu, L.; Nix, W. D.; Cui, Y. Interconnected Silicon Hollow Nanospheres for Lithium-Ion Battery Anodes with Long Cycle Life. *Nano Lett.* **2011**, *11*, 2949−2954.

(10) Chan, C. K.; Peng, H.; Liu, G.; Mcllwrath, K.; Zhang, X. F.; Huggins, R. A.; Cui, Y. High-Performance Lithium Battery Anodes Using Silicon Nanowires. *Nat. Nanotechnol.* **2008**, *3*, 31−35.

(11) Cui, L.-F.; Ruffo, R.; Chan, C. K.; Peng, H.; Cui, Y. Crystalline-Amorphous Core-Shell Silicon Nanowires for High Capacity and High Current Battery Electrodes. *Nano Lett.* **2009**, *9*, 491−495.

(12) Song, T.; Xia, J.; Lee, J.-H.; Lee, D. H.; Kwon, M.-S.; Choi, J.-M.; Wu, J.; Doo, S. K.; Chang, H.; Park, W. I.; et al. Arrays of Sealed Silicon Nanotubes as Anodes for Lithium Ion Batteries. *Nano Lett.* **2010**, *10*, 1710−1716.

(13) Wu, H.; Chan, G.; Choi, J. W.; Ryu, L.; Yao, Y.; McDowell, M. T.; Lee, S. W.; Jackson, A.; Yang, Y.; Hu, L.; et al. Stable Cycling of Double-Walled Silicon Nanotube Battery Anodes through Solid−Electrolyte Interphase Control. *Nat. Nanotechnol.* **2012**, *7*, 310−315.

(14) Hwang, T. H.; Lee, Y. M.; Kong, B.-S.; Seo, J.-S.; Choi, J. W. Electrospun Core−Shell Fibers for Robust Silicon Nanoparticle-Based Lithium Ion Battery Anodes. *Nano Lett.* **2012**, *12*, 802−807.

(15) Liu, X. H.; Zhong, L.; Huang, S.; Mao, S. X.; Zhu, T.; Huang, J. Y. Size-Dependent Fracture of Silicon Nanoparticles during Lithiation. *ACS Nano* **2012**, *6*, 1522−1531.

(16) Wen, Z. S.; Yang, J.; Wang, B. F.; Wang, K.; Liu, Y. High Capacity Silicon/Carbon Composite Anode Materials for Lithium Ion Batteries. *Electrochem. Commun.* **2003**, *5*, 165−168.

(17) Wang, B.; Li, X.; Qiu, T.; Luo, B.; Ning, J.; Li, J.; Zhang, X.; Liang, M.; Zhi, L. High Volumetric Capacity Silicon-Based Lithium Battery Anodes by Nanoscale System Engineering. *Nano Lett.* **2013**, *13*, 5578−5584.

(18) Persson, K.; Sethuraman, V. A.; Hardwick, L. J.; Hinuma, Y.; Meng, Y. S.; van der Ven, A.; Srinivasan, V.; Kostecki, R.; Ceder, G. Lithium Diffusion in Graphitic Carbon. *J. Phys. Chem. Lett.* **2010**, *1*, 1176−1180.

(19) Kim, H.; Kweon, K. E.; Chou, C.-Y.; Ekerdt, J. G.; Hwang, G. S. On the Nature and Behavior of Li Atoms in Si: A First Principles Study. *J. Phys. Chem. C* **2010**, *114*, 17942−17946.

(20) Chou, C.-Y.; Kim, H.; Hwang, G. S. A Comparative First-Principles Study of the Structure, Energetics, and Properties of Li-M (M = Si, Ge, Sn) Alloys. *J. Phys. Chem. C* **2011**, *115*, 20018−20026.

(21) Zhang, Q.; Zhang, W.; Wan, W.; Cui, Y.; Wang, E. Lithium Insertion in Silicon Nanowires: An Ab Initio Study. *Nano Lett.* **2010**, *10*, 3243−3249.

(22) Chon, M. J.; Sethuraman, V. A.; McCormick, A.; Srinivasan, V.; Guduru, P. R. Real-Time Measurement of Stress and Damage Evolution during Initial Lithiation of Crystalline Silicon. *Phys. Rev. Lett.* **2011**, *107*, 045503(1)−045503(4).

(23) Liu, X. H.; Zheng, H.; Zhong, L.; Huang, S.; Karki, K.; Zhang, L. Q.; Liu, Y.; Kushima, A.; Liang, W. T.; Wang, J. W.; et al. Anisotropic Swelling and Fracture of Silicon Nanowires during Lithiation. *Nano Lett.* **2011**, *11*, 3312−3318.

(24) Kim, H.; Chou, C.-Y.; Ekerdt, J. G.; Hwang, G. S. Structure and Properties of Li-Si Alloys: A First-Principles Study. *J. Phys. Chem. C* **2011**, *115*, 2514−2521.

(25) Lee, S. W.; McDowell, M. T.; Choi, J. W.; Cui, Y. Anomalous Shape Changes of Silicon Nanopillars by Electrochemical Lithiation. *Nano Lett.* **2011**, *11*, 3034−3039.

(26) Lee, S. W.; McDowell, M. T.; Berla, L. A.; Nix, W. D.; Cui, Y. Fracture of Crystalline Silicon Nanopillars during Electrochemical Lithium Insertion. *Proc. Natl. Acad. Sci. U.S.A.* **2012**, *109*, 4080−4085.

(27) Liu, X. H.; Wang, J. W.; Huang, S.; Fan, F.; Huang, X.; Liu, Y.; Krylyuk, S.; Yoo, J.; Dayeh, S. A.; Davydov, A. V.; et al. In Situ Atomic-Scale Imaging of Electrochemical Lithiation in Silicon. *Nat. Nanotechnol.* **2012**, *7*, 749−756.

(28) Key, B.; Bhattacharyya, R.; Morcrette, M.; Seznéc, V.; Tarascon, J.-M.; Grey, C. P. Real-Time NMR Investigations of Structural Changes in Silicon Electrodes for Lithium-Ion Batteries. *J. Am. Chem. Soc.* **2009**, *131*, 9239−9249.

(29) Key, B.; Morcrette, M.; Tarascon, J.-M.; Grey, C. P. Pair Distribution Function Analysis and Solid State NMR Studies of Silicon Electrodes for Lithium Ion Batteries: Understanding the (De)lithiation Mechanisms. *J. Am. Chem. Soc.* **2011**, *133*, 503−512.

(30) Ogata, K.; Salager, E.; Kerr, C. J.; Fraser, A. E.; Ducati, C.; Morris, A. J.; Hofmann, S.; Grey, C. P. Revealing Lithium−Silicide Phase Transformations in Nano-Structured Silicon-Based Lithium Ion Batteries via In Situ NMR Spectroscopy. *Nat. Commun.* **2014**, *5*, 3217(1)−3217(11).

(31) Johari, P.; Qi, Y.; Shenoy, V. B. The Mixing Mechanism during Lithiation of Si Negative Electrode in Li-Ion Batteries: An Ab Initio Molecular Dynamics Study. *Nano Lett.* **2011**, *11*, 5494−5500.

(32) Wang, Z.; Gu, M.; Zhou, Y.; Zu, X.; Connell, J. G.; Xiao, J.; Perea, D.; Lauhon, L. J.; Bang, J.; Zhang, S.; et al. Electron-Rich Driven

DOI: 10.1021/jp5094756
J. Phys. Chem. C 2015, 119, 3447−3455

Electrochemical Solid-State Amorphization in Li−Si Alloys. *Nano Lett.* **2013**, *13*, 4511−4516.
(33) Chan, M. K. Y.; Wolverton, C.; Greeley, J. P. First Principles Simulations of the Electrochemical Lithiation and Delithiation of Faceted Crystalline Silicon. *J. Am. Chem. Soc.* **2012**, *134*, 14362−14374.
(34) Zhao, K.; Wang, W. L.; Gregoire, J.; Pharr, M.; Suo, Z.; Vlassak, J. J.; Kaxiras, E. Lithium-Assisted Plastic Deformation of Silicon Electrodes in Lithium-Ion Batteries: A First-Principles Theoretical Study. *Nano Lett.* **2011**, *11*, 2962−2967.
(35) Jung, S. C.; Choi, J. W.; Han, Y.-K. Anisotropic Volume Expansion of Crystalline Silicon during Electrochemical Lithium Insertion: An Atomic Level Rationale. *Nano Lett.* **2012**, *12*, 5342−5347.
(36) Cubuk, E. D.; Wang, W. L.; Zhao, K.; Vlassak, J. J.; Suo, Z.; Kaxiras, E. Morphological Evolution of Si Nanowires upon Lithiation: A First- Principles Multiscale Model. *Nano Lett.* **2013**, *13*, 2011−2015.
(37) Yang, H.; Huang, S.; Huang, X.; Fan, F.; Liang, W.; Liu, X. H.; Chen, L.-Q.; Huang, J. Y.; Li, J.; Zhu, T.; et al. Orientation-Dependent Interfacial Mobility Governs the Anisotropic Swelling in Lithiated Silicon Nanowires. *Nano Lett.* **2012**, *12*, 1953−1958.
(38) van Duin, A. C. T.; Dasgupta, S.; Lorant, F.; Goddard, W. A., III. ReaxFF: A Reactive Force Field for Hydrocarbons. *J. Phys. Chem. A* **2001**, *105*, 9396−9409.
(39) van Duin, A. C. T.; Strachan, A.; Stewman, S.; Zhang, Q.; Xu, X.; Goddard, W. A., III. $ReaxFF_{SiO}$ Reactive Force Field for Silicon and Silicon Oxide Systems. *J. Phys. Chem. A* **2003**, *107*, 3803−3811.
(40) Han, S. S.; van Duin, A. C. T.; Goddard, W. A., III.; Lee, H. M. Optimization and Application of Lithium Parameters for the Reactive Force Field, ReaxFF. *J. Phys. Chem. A* **2005**, *109*, 4575−4582.
(41) Han, S. S.; Kang, J. K.; Lee, H. M.; van Duin, A. C. T.; Goddard, W. A., III. The Theoretical Study on Interaction of Hydrogen with Single-Walled Boron Nitride Nanotubes. I. The Reactive Force Field $ReaxFF_{HBN}$ Development. *J. Chem. Phys.* **2005**, *123*, 114703(1)−114703(8).
(42) van Duin, A. C. T.; Merinov, B. V.; Han, S. S.; Dorso, C. O.; Goddard, W. A., III. ReaxFF Reactive Force Field for the Y-Doped $BaZrO_3$ Proton Conductor with Applications to Diffusion Rates for Multigranular Systems. *J. Phys. Chem. A* **2008**, *112*, 11414−11422.
(43) Bedrov, D.; Smith, G. D.; van Duin, A. C. T. Reactions of Singly-Reduced Ethylene Carbonate in Lithium Battery Electrolytes: A Molecular Dynamics Simulation Study Using the ReaxFF. *J. Phys. Chem. A* **2012**, *116*, 2978−2985.
(44) Fan, F.; Huang, S.; Yang, H.; Raju, M.; Datta, D.; Shenoy, V. B.; van Duin, A. C. T.; Zhang, S.; Zhu, T. Mechanical Properties of Amorphous Li_xSi Alloys: A Reactive Force Field Study. *Modell. Simul. Mater. Sci. Eng.* **2013**, *21*, 074002(1)−074002(15).
(45) Kim, S.-P.; Datta, D.; Shenoy, V. B. Atomistic Mechanisms of Phase Boundary Evolution during Initial Lithiation of Crystalline Silicon. *J. Phys. Chem. C* **2014**, *118*, 17247−17253.
(46) Plimpton, S. Fast Parallel Algorithms for Short-Range Molecular Dynamics. *J. Comput. Phys.* **1995**, *117*, 1−19.
(47) Verlet, L. Computer "Experiments" on Classical Fluids. I. Thermodynamical Properties of Lennard-Jones Molecules. *Phys. Rev.* **1967**, *159*, 98−103.
(48) Hoover, W. G. Canonical Dynamics: Equilibrium Phase-Space Distributions. *Phys. Rev. A* **1985**, *31*, 1695−1697.
(49) Peng, B.; Cheng, F.; Tao, Z.; Chen, J. Lithium Transport at Silicon Thin Film: Barrier for High-Rate Capability Anode. *J. Chem. Phys.* **2010**, *133*, 034701(1)−034701(5).
(50) Cubuk, E. D.; Kaxiras, E. Theory of Structural Transformation in Lithiated Amorphous Silicon. *Nano Lett.* **2014**, *14*, 4065−4070.
(51) Zhou, G. W.; Li, H.; Sun, H. P.; Yu, D. P.; Wang, Y. Q.; Huang, X. J.; Chen, L. Q.; Zhang, Z. Controlled Li Doping of Si Nanowires by Electrochemical Insertion Method. *Appl. Phys. Lett.* **1999**, *75*, 2447−2449.
(52) Li, H.; Huang, X.; Chen, L.; Zhou, G.; Zhang, Z.; Yu, D.; Mo, Y. J.; Pei, N. The Crystal Structural Evolution of Nano-Si Anode Caused by Lithium Insertion and Extraction at Room Temperature. *Solid State Ionics* **2000**, *135*, 181−191.
(53) Kang, K.; Lee, H.-S.; Han, D.-W.; Kim, G.-S.; Lee, D.; Lee, G.; Kang, Y.-M.; Jo, M.-H. Maximum Li Storage in Si Nanowires for the High Capacity Three-Dimensional Li-Ion Battery. *Appl. Phys. Lett.* **2010**, *96*, 053110(1)−053110(3).
(54) Gu, M.; Wang, Z.; Connell, J. G.; Perea, D. E.; Lauhon, L. J.; Gao, F.; Wang, C. Electronic Origin for the Phase Transition from Amorphous Li_xSi to Crystalline $Li_{15}Si_4$. *ACS Nano* **2013**, *7*, 6303−6309.

DOI: 10.1021/jp5094756
J. Phys. Chem. C 2015, 119, 3447−3455